SAND2021-9207J

Load Dynamics of Double Planar Foil Liners and Double Planar Wire Arrays on the UM MAIZE LTD Generator

C.J. Butcher[1], V.L. Kantsyrev[1], A.S. Safronova[1], V.V. Shlyaptseva[1], I.K. Shrestha[1], A. Stafford[1], A.M. Steiner[2], P.C. Campbell[3], S.M. Miller[3], D. Yager-Elorriaga[2], N.M. Jordan[3], R.D. McBride[3], R.M. Gilgenbach[3]

[1]*Physics Department, University of Nevada, Reno, NV 89557, USA*
[2]*Sandia National Laboratories, Albuquerque, NM 87110, USA*
[3]*Plasma, Pulsed Power, and Microwave Laboratory, Department of Nuclear Engineering and Radiological Sciences, University of Michigan, Ann Arbor, Michigan 48109, USA*

Author to whom correspondence should be addressed: christopherbutcher@nevada.unr.edu

Abstract

In previous studies using UNR's high-impedance Zebra Marx generator (1.9 Ω, 1.7 MA, 100 ns), Double Planar Wire Arrays (DPWAs) proved to be excellent radiators, and Double Planar Foil Liners (DPFLs) proved useful for future ICF applications. This article presents the results of joint UNR/UM experiments with Aluminum (Al) DPWAs, Al DPFLs, and Tungsten (W) DPWAs using UM's MAIZE generator, a low-impedance Linear Transformer Driver (LTD) (0.1 Ω, 0.5–1 MA, and 100–250 ns). The main goals of this study were twofold: the first was a pioneering effort to test if a relatively heavy Al DPFL could be successfully imploded on a low-impedance University-scale LTD like the MAIZE generator, and, if so, to analyze the results and make comparisons to the optimized, lighter DPWA configurations that have been studied previously. The DPWAs consisted of two planes of micron-scale diameter Al or W wires, while the DPFLs consisted of two planes of micron-scale thickness Al foils. Diagnostics include filtered Si-diodes, an absolutely calibrated filtered PCD, x-ray pinhole cameras, spectrometers, and gated optical self-emission imaging. The implosion dynamics and radiative properties of Al DPWAs and DPFLs and W DPWAs on the MAIZE LTD are discussed and compared. Time-dependent load inductance calculations derived from measurements of the load current and a MAIZE circuit model provide a relative measurement of pinch strength. In experiments on MAIZE, W planar wire arrays exhibited a higher peak load inductance throughout the pinch than Al DPWAs and DPFLs, while x-ray pulses from Al DPFLs had the longest emission duration.

I. Introduction

The plasma dynamics of implosions on pulsed power machines is heavily dependent upon the current carrying load type and configuration used. Planar Wire Arrays (PWAs) [Single Planar Wire Arrays (SPWAs) and Double Planar Wire Arrays (DPWAs, see Fig. 1A)] have proven to be excellent x-ray radiators on both university scale pulsed power generators [1] and at Sandia National Laboratories (SNL) on the multi-MA Saturn machine [2]. Among the loads tested on the UNR Zebra generator, planar wire arrays (PWA) were found to be the most efficient compact x-ray radiators at the 1–2 MA scale [1, 3, 4]. In comparison with cylindrical wire arrays (CWA), the PWA is characterized by a unique combination of: (1) larger resistive energy deposition [1]; (2) higher radiated output powers [1, 3, 4]; (3) small (mm) scale size [1, 5]; (4) the possibility of radiation pulse shaping [6]; (5) the ability to study plasma flows and spectroscopy from two and even three planes of different wire materials in one shot [7, 8]; and (6) overall good diagnostics access to inner plasmas [1]. As an example of the efficient radiation output, DPWAs (particularly those made from tungsten or other mid-atomic-number elements) have demonstrated radiation pulses of up to 30 kJ and >1 TW on the UNR Zebra generator, which stores 150 kJ in its capacitor banks [9]. In addition to being excellent radiators of x-rays, PWA sources have applications in inertial confinement fusion (including the new compact multisource hohlraum design [2, 4]), astrophysical studies [10], and lasing research [11].

As a possible alternative to PWAs and CWAs on future >30-MA generators, Planar Foil Liners (PFLs, see Fig. 1B) have been proposed. The continuous foil load is thought to be a useful replacement for discrete wires at >30-MA current levels because when the CWAs and/or PWAs are scaled to such currents, the inter-wire gap spacing decreases, and the coronal plasma surrounding each individual wire expands and significantly overlaps with the coronal plasmas from neighboring wires [5]. Previously, encouraging results with Double Planar Foil Liners (DPFLs, see Fig. 1B) have been obtained in experiments using the high-impedance UNR Marx bank Zebra generator [5, 12], where it was found that the Al DPFL electron temperature (T_e), electron density (n_e), and x-ray yield were comparable to Al DPWAs with similar mass. However, almost no data on DPFL x-ray sources has been collected on low-impedance drivers, such as a single-cavity Linear Transformer Driver (LTD). As a result, very little is known about the implosion and radiative performance of these load types on low-impedance drivers.

Low-impedance LTD accelerators are a relatively new technology, and they have been theorized to be capable of reaching higher currents and powers more efficiently than the widely-used Marx-driven generators. Because of this, LTDs have been proposed for future petawatt-class Z-pinch generator designs [13, 14]. Recently, Al DPWAs were successfully

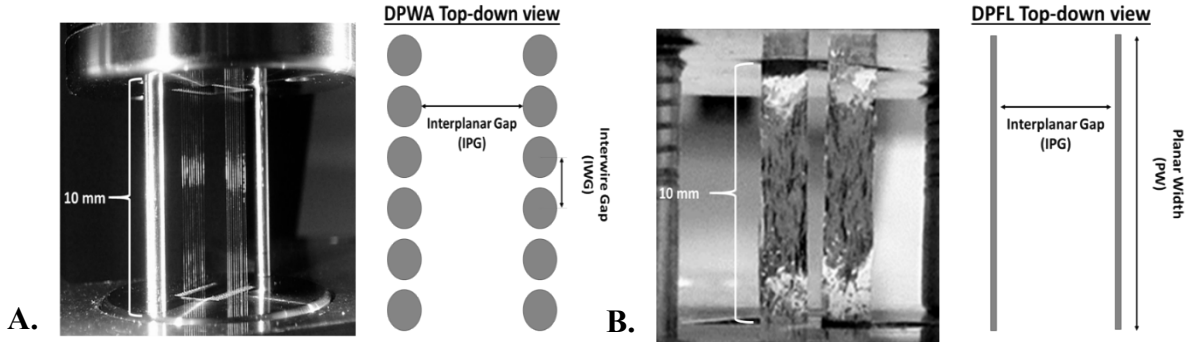

Figure 1. An example of an Al DPWA load (A, left) and an Al DPFL load (B, right) with accompanying top down schematic views showing the Interplanar Gap (IPG) and Interwire Gap (only for DPWA) and the Planar Width (shown on DPFL). The supporting rods are removed prior to the shot.

imploded on the low-impedance (0.1 Ω), low-stored-energy (7.8 kJ at ±70-kV charge voltage) MAIZE LTD at the University of Michigan [15]. By contrast, this paper presents the first experimental results of DPFL implosions on the low-impedance MAIZE facility. The DPFL results obtained on MAIZE are compared to the more well understood Al DPWAs and W DPWAs configurations on MAIZE [15, 16] and to Al DPFLs on the Zebra generator [5, 7].

II. Experimental Details

Experiments were performed using the Michigan Accelerator for Inductive Z-Pinch Experiments (MAIZE) at UM, which is a single-cavity Linear Transformer Driver (LTD) [17]. MAIZE is a single-stage, low impedance (0.1 Ω), 1 MA class LTD with 100 ns risetime into an impedance matched load. The load is housed in the center of a circular, 1-m-diameter vacuum chamber located in the center of the 3-m-diameter cavity. Experimental diagnostics were located inside and outside the vacuum chamber. The setup inside the chamber is shown in Fig. 2. Diagnostics included various filtered x-ray diodes; x-ray spectrometers and x-ray pinhole cameras; a filtered Faraday cup placed above the load for measurement of the electron beam [15]; an ultra-fast, intensified, 12-frame camera for use in shadowgraphy/self-emission imaging; and B-dot loops at four azimuthal locations on the radial transmission line for measurement of the time-resolved current pulse. Results of electron beam measurements made with the Faraday Cup above the anode will be the subject of a future publication.

The time-resolved x-ray output throughout each shot was measured using a side-on absolutely calibrated photoconducting diamond detector (PCD) with a time resolution of 0.5 ns. The PCD was filtered to detect photons with energies above a cutoff energy of 2.4 keV. The cutoff energy E is defined as the energy where the transmission through the filter drops to a value of 1/e, where e is the base of the natural logarithm. Three side-on, cross-calibrated AXUV-HS5 Si-diodes with a time resolution of 1 ns and filtered to detect >1.4, >3.5, and >9 keV x-rays were also used to measure the time-evolution of the x-ray output in different energy bands. All of these diode detectors were placed such that the line of sight would be within 15° or less, with respect to the planes of the arrays for DPWAs and DPFLs (i.e. the line of sight that looks into the gap between the planes). The oscilloscopes used featured a sample rate of 5 GS/s, capable of resolving the PCD time resolution.

The two side-on x-ray pinhole cameras (spatial resolution of 90 μm) were placed approximately 90° apart from each other to view the load from both the "front" and "side" view; the first was placed within 15° or less, with respect to the planes of the arrays, while the second was placed at approximately 95°-105°. Each pinhole was capable of taking three independent, time-integrated x-ray images (filtered to detect >1.4, >1.6, and >3.5 keV x-rays) onto Kodak Biomax MS X-ray film, with grain size 0.12±0.03 μm [18]; the use of this film for x-ray imaging and spectroscopic measurements is discussed in detail in Ref. [19]. Two side-on time-integrated x-ray spectrometers were applied to estimate electron temperature (T_e), electron density (n_e), and opacity effects of the Al Z-pinch plasmas, using non-local thermal equilibrium (non-LTE) kinetic models [15, 20]. The two spectrometers were employed to measure x-rays in two different x-ray bands: a softer x-ray spectral region between 4 and 13 Å and a harder region between 1 and 2.4 Å. The softer x-ray spectrometer had a convex potassium acid phthalate (KAP) crystal with a double lattice spacing 2d = 26.63 Å, a radius of curvature of 51 mm, a 1-D axial spatial resolution of 4 mm, and a spectral resolution $R=\lambda/\Delta\lambda=500$. The harder x-ray spectrometer had a convex lithium fluoride (LiF) crystal with a double lattice spacing 2d = 4.027 Å, a radius of curvature of 25.4 mm, and a 1-D axial spatial resolution of 4

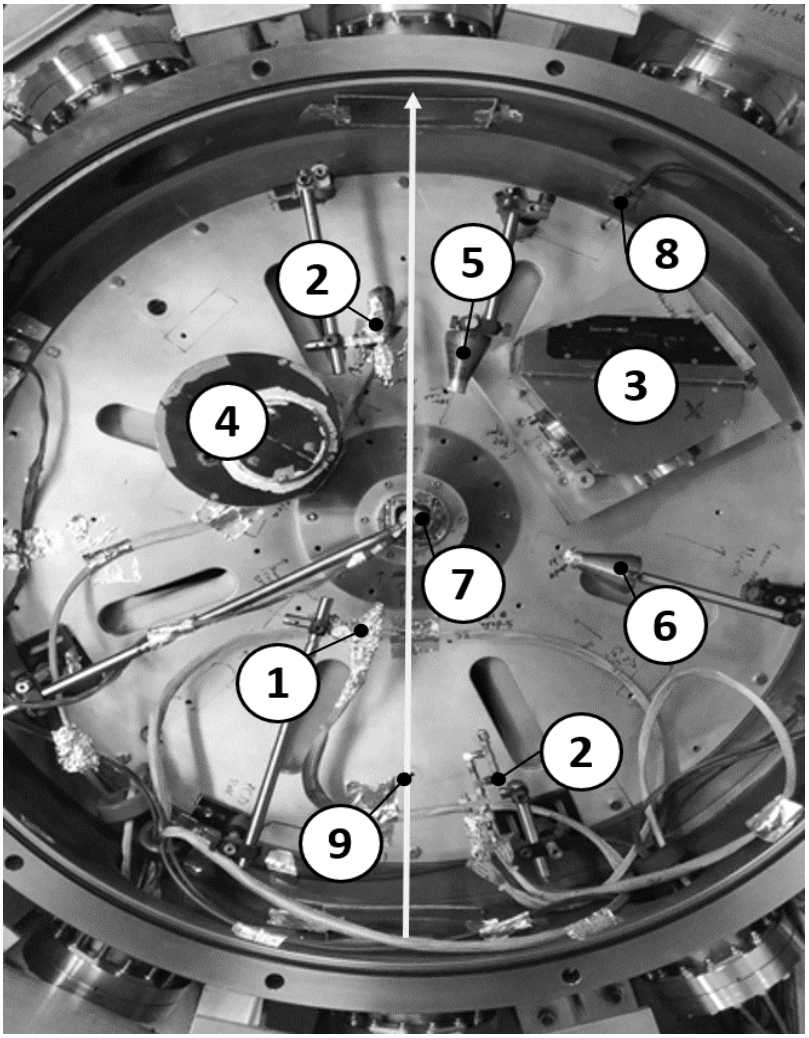

Figure 2. Top-down view of the MAIZE vacuum chamber with X-ray and electron beam diagnostics surrounding the centrally located DPWA load: (1) x-ray PCD; (2) Si diodes; (3) soft X-ray KAP-crystal spectrometer; (4) hard X-ray LiF-crystal spectrometer; (5) x-ray pinhole camera placed along the load wire planes; (6) x-ray pinhole camera placed orthogonal to the wire planes; (7) Faraday cup detector placed above the load in the center of the chamber; (8) B-dot sensors placed along the edges of the chamber 90° from each other (not all B-dot sensors are visible in this image); (9) grey arrow representing the optical probing beam path/camera line of sight through the chamber and load.

mm. The spectrometers were equipped with 7.5-μm-thick Kapton film together with 3-μm-thick Mylar (aluminized on both sides with 0.15-μm-thick Al layers) to protect the inside film from unwanted outside light. Previous results of these diagnostics are discussed in detail in Refs. [15, 16].

An intensified, ultra-fast 12-frame camera was employed to collect self-emission images prior to and throughout the Z-pinching process to study the plasma evolution. In previous experiments, this ultra-fast camera was paired with a 532-nm, 2-ns, frequency doubled Nd:YAG pulse, split into optical beams with a 10 ns delay between each beam for use as a backlighting source for shadowgraphy images [21]. Shadowgraphy images of DPWA implosions on MAIZE are presented in Refs. [15, 16]. For self-emission imaging, shots were performed without the laser backlighting, and the images taken were only of the light emitted by the Z-pinching load. Previous experiments using cylindrical foil liners on MAIZE showed only small variations in the observation of the plasma-vacuum boundary between self-emission

and laser-backlit shots [22, 23]. All of the MAIZE shots analyzed in this manuscript were imaged using the self-emission method with 10 ns exposure per frame.

Four B-dot probes, radially located approximately 0.4 m from the load at the center of the chamber and equally spaced azimuthally (90° between adjacent probes) were used to measure the time-resolved current trace throughout the Z-pinch. As the MAIZE LTD is a low-impedance machine, the change in inductance of the plasma load throughout the Z-pinching process has a larger effect on the current trace compared to stiff (high impedance) drivers like the Zebra Marx generator at UNR. The effect that the load inductance has on the current trace can be explored by comparing the measured current trace to a simulated, static inductance (non-imploding) load to calculate an effective inductance of the load throughout the Z-pinch as a function of time. This method is explained in detail in Ref. [24] and is expanded in Section IV to more closely approximate the time-dependent load inductance.

In these experiments, the DPWAs consisted of two parallel wire planes, while the DPFLs consisted of two parallel foil planes. The DPWA masses were calculated from the number of wires, the diameter of the wires, and the wire material, while the DPFL masses were calculated from the width of the foil, the thickness of the foil, and the foil material. In Ref. [6], it was observed that DPWA implosion dynamics depend strongly upon the aspect ratio φ, defined as the ratio of the array width to the inter-planar gap. In the following sections, we present results from two DPWAs (one made of 5-μm-diameter W wires, and another made of 12.7-μm-diameter Al wires) and one DPFL (made of 1.8-μm-thick Al foil) imploded using the MAIZE LTD generator. The anode-cathode gap was 1 cm for both the DPWAs and the DPFLs, while the inter-wire spacing was 0.7 mm for the DPWAs.

Due to the relatively large inductance of the DPWA/DPFL load hardware, the MAIZE LTD was limited to 70% of the maximum charge voltage in an effort to prevent damage to the main (central) insulator and to minimize voltage reversal on the capacitors. Under such operating conditions, the peak current was typically between 450 kA - 600 kA and the risetime ranged from 200 - 300 ns.

III. Radiative Properties of Al DPFLs, Al DPWAs, and W DPWAs on the MAIZE LTD

IIIa. Radiative Properties of Al DPFLs on the MAIZE LTD

During these experiments, a relatively massive Al DPFL was imploded (340 μg/cm).

Multiple shots with this load were conducted to understand the reproducibility of the implosion.

The DPFL data presented have been selected from these shots to best represent the DPFL

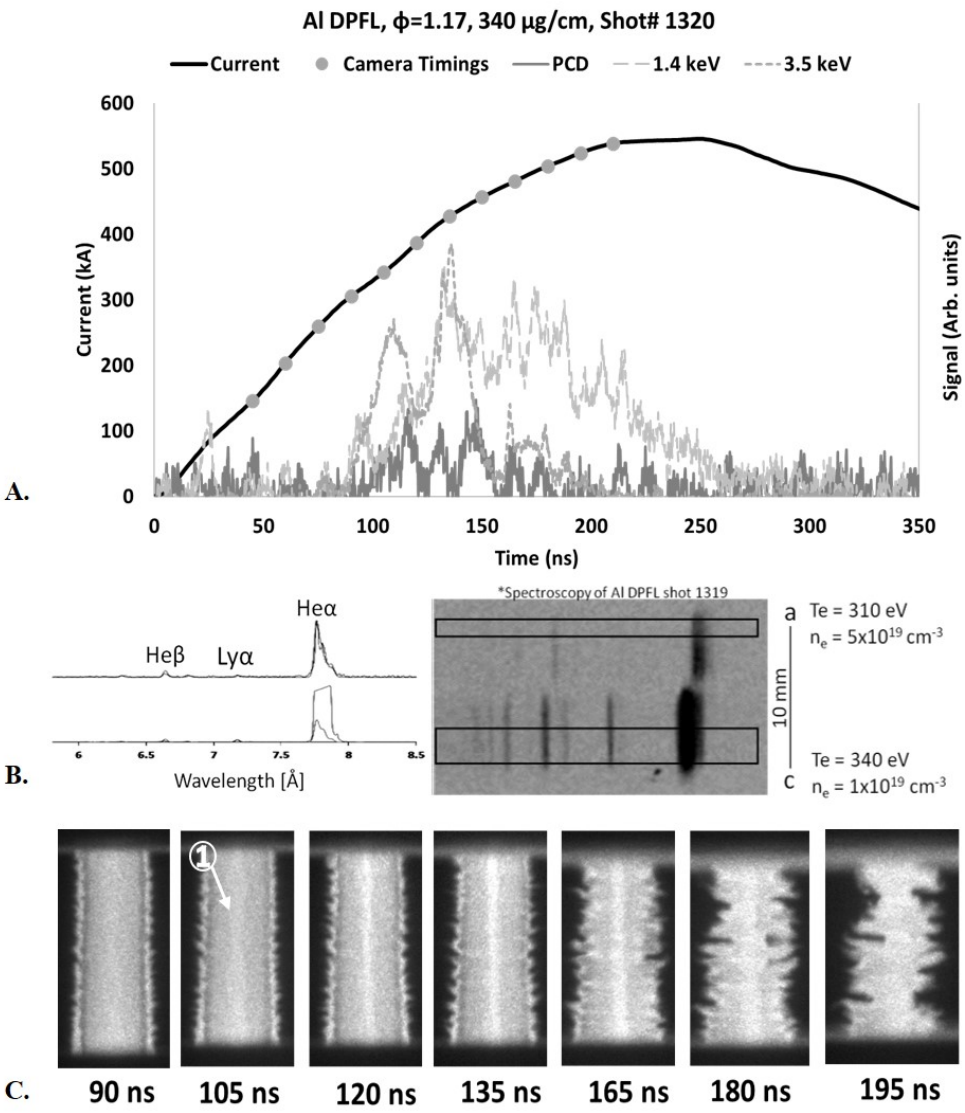

Figure 3. Al DPFLs on MAIZE. A. Radiation output from MAIZE Shot 1320 (inter-planar gap = 3 mm, planar width = 3.5 mm, aspect ratio ϕ=1.17, mass = 340 µg/cm). The PCD signal (dark grey) shows radiation in the >2.4 keV region, while the Si-diode signals (light grey long dashes and grey dashes) shows radiation signals in >1.4 and >3.5 keV spectral bands, respectively. Current (black) risetime was 250 ns with the major implosion occurring at 135-145 ns from the start of current. Grey dots correspond to moments when a self-emission image was taken. B. MAIZE Shot 1319 (an identical load configuration to Shot 1320). The 1D spatially resolved, time integrated X-ray spectra are compared to theoretical modelling to find plasma conditions. C. Self-emission images from MAIZE Shot 1320 shows the implosion evolution in time from the start of current. Formation and position of the primary precursor column is marked by "1."

implosion. As can be seen in Fig. 3, the Al DPFLs generated radiation bursts throughout the implosion. The radiation output from the Al DPFLs are characterized by longer lasting bursts compared to the mass-optimized Al DPWA and the W DPWA on MAIZE, which will be discussed later. The most intense radiation bursts from the Al DPFL were measured to last approximately 70 ns for the >3.5 keV band and much longer (about 160 ns) for the >1.4 keV band. Three distinct peaks can be seen in the PCD signal, occurring between 100 and 150 ns, as well as two smaller peaks from 150-180 ns that concur with noticeable peaks in the >3.5 keV signal. Another interesting observation to note is that the load began radiating shortly after the start of the current pulse (approximately 80 ns) and long before peak current occurred at approximately 250 ns.

The initial x-ray burst measured from the radiation signals (Fig. 3A) occurs simultaneously with a significant increase in the brightness of the central column seen in the self-emission images (Fig. 3C) at 105-120 ns. Likewise, the second and most powerful burst occurs shortly after at 130-140 ns, followed by two smaller bursts at 155-165 and 175-185 ns. The load continues to produce measurable x-ray signal up to 250 ns after the start of current. Altogether, the Al DPFL demonstrates a longer, more drawn-out pinch process, with multiple radiation peaks, than is typically observed in DPWA configurations tested on MAIZE, which typically demonstrate a more definable peak of x-ray emission. This may be due to the additional mass of the DPFL (relative to the less massive DPWAs tested on MAIZE). As can be observed in the self-emission images, mass accumulation along the central axis formed a central "precursor" column at 90-105 ns. However, no standing shocks appear to have formed by this time (see Fig. 4c and Fig. 5c in this paper, and Fig. 5 in Ref. [16] for images of standing shocks, as well as Ref. [6] for a detailed explanation of how they form); instead, a steady stream of mass continuously contributed to the central plasma column. This drawn-out z-pinching process is also likely enhanced by MAIZE's relatively high sensitivity to changes in load inductance throughout the process. That is, as the precursor plasma is advected to the central column, some of the drive current is likely transported to the column as well. This makes the load more inductive, which reduces the drive on the remaining foil material and thus extends the time required to implode the bulk of the foil material. This phenomenon will be addressed in more detail in Section IV when discussing the inductance modelling.

As is understood for DPWA implosions, due to the initial current distribution through the load, the outer wires ablate first [1, 6, 15]. Similarly, it is believed that the outer regions of the foil planes will ablate prior to the inner parts of the foil planes. This was modelled in Ref. [1], which showed preliminary calculations for a double planar load with an even mass distribution, analogous to a foil plane. As such, with the heavy mass of the DPFL, the material on the outer parts of the foil planes likely imploded and pinched earlier than the inner parts of the foil planes. With the higher mass of the DPFL, this process is extended in time, leading to the longer radiation period observed (relative to the less massive DPWAs tested on MAIZE). The radiation waveforms presented in Fig. 3 (with multiple bursts spread out in time) are similar to those observed for DPFL shots on Zebra (see Ref. [5]), which demonstrated a higher number of radiation bursts spread out over a longer duration in time when compared to DPWA shots on the same generator, albeit with a shorter overall pinching time than on MAIZE (60 ns on Zebra versus 150 ns on MAIZE).

Using spatially resolved spectroscopic analysis, including modelling of K-shell Al transitions from the high Rydberg states for the Al DPFL [15, 20], the electron temperature (T_e) and density (n_e) were modeled near the anode and cathode (Fig. 3B): T_e was 310 eV, n_e was 5 x 10^{19} cm^{-3} near the anode, and T_e was 340 eV, n_e was 10^{19} cm^{-3} near the cathode. Also, the modeling indicated an optically thin plasma near the anode (Fig. 3B), which is very unusual for pulsed power Al plasmas on Zebra.

IIIb. Radiative Properties of Al DPWAs on the MAIZE LTD

For comparison, less massive Al DPWAs (41-76 μg/cm) were also imploded on the MAIZE LTD generator. MAIZE Shot 1315 was selected for analysis as it demonstrated the most pronounced and integrable signal on the PCD, such that the overall energy output could be measured (see Table 1). Additionally, a shot featuring an identical load configuration was modeled in Ref. [15] using the Wire Ablation Dynamics Model (WADM) [25, 26]. In contrast to the more massive Al DPFL, the less massive Al DPWA showed a more typical radiation burst behavior (Fig. 4A); however, the main burst still occurred prior to peak

current (at 205-215 ns). The total x-ray duration (which includes multiple bursts) is 35-45 ns. The main x-ray burst (i.e., the first burst, which is less than 5 ns in duration) was followed by two smaller bursts at 225 ns and 235 ns. These subsequent bursts had peak magnitudes that were ~1/3 of that from the main burst, as measured in both the >2.4 keV band (PCD) and the >3.5 keV band (Si-diode). There is a small amount of radiation in the >3.5 keV region beginning at 80-90 ns, which coincides with the early formation of standing shocks appearing in Fig. 4C. These shocks are the bright structures that appear in the 95 and 125-ns frames of Fig. 4C.

MAIZE Shot	Material	Load	Aspect Ratio	Mass (μg/cm)	Current Max (kA)	Current Risetime (ns)	Implosion Time (ns)	Energy over 4π (J)	Conversion Factor ε
1315	Al	DPWA	0.58	41	585	260	220	6.7E-02	8.5E-06
1320	Al	DPFL	1.17	340	565	215	140	3.3E-02	4.2E-06
1334	W	DPWA	1.05	76	475	200	245	1.6E+00	2.1E-04

Table 1. Experimental parameters tested on MAIZE. The implosion times are measured relative to the start of the current pulse. The radiated energies are for the >2.4 keV band, integrated over the duration of the experiment. The error in energy calculations was 35% [16]. Issues with LTD switch firing times and inconsistent B-dot probe readings led to an estimated error of approximately 50 kA in the maximum currents listed.

Further observations of the self-emission images in Fig. 4C show that around 155-185 ns, the two independent plasma flows begin to merge along the central axis, forming the precursor plasma column. The formation of a precursor column is rare for DPWA loads with such low aspect ratios ($\varphi<0.7$); this phenomenon was first reported on the MAIZE LTD in Ref. [13]. The main z-pinch begins around 215 ns, after the wire material has fully ablated and is flowing towards the central column, which corresponds well in time with the main radiation burst. Spectroscopic analysis of the Al DPWA shows that near the anode, T_e was 380 eV and n_e was 10^{19} cm^{-3}, while near the cathode, T_e was 375 eV and n_e was 3 x 10^{19} cm^{-3} (see Fig. 4B).

The x-ray yields of both the more massive Al DPFL and the less massive Al DPWA were approximated by integrating the signals from the absolutely calibrated PCD over the entire duration of emission and assuming isotropic radiation into 4π steradians. The anisotropic distribution of total x-rays for DPWAs was found to be small (~10-20%) for similar DPWA configurations [27]. The Conversion Factor (ε), defined as the ratio of the total x-ray output in a certain energy range (>2.4 keV in this work) to the energy initially stored in the generator capacitors (7.8 kJ in this work), is a measurement of the efficiency of the machine. As shown in Table 1, the x-ray yield in the >2.4 keV band of the more massive Al DPFL was 3.3 x 10^{-2} J, and thus $\varepsilon_{\text{Al DPFL}}$ = 4.2 x 10^{-6}, while the optimized, less massive Al DPWA was only twice as large at 6.7 x 10^{-2} J, and thus $\varepsilon_{\text{Al DPWA}}$ = 8.5 x 10^{-6}. This is an intriguing result, as the mass optimized DPWA only outperformed the much heavier DPFL by a factor of two. This could imply that a mass optimized DPFL could match or possibly outperform a DPWA of similar mass on the MAIZE LTD. The experimental error in the total x-ray output was 35% [16].

Spectroscopic modelling of both the Al DPFLs and DPWAs showed comparable electron temperature (T_e) and density (n_e): T_e^{DPFL} = 310-340 eV, n_e^{DPFL} = (1-5) x 10^{19} cm^{-3} (I = 0.56 MA), and T_e^{DPWA} = 375-380 eV, n_e^{DPWA} = (1-3) x 10^{19} cm^{-3} (I = 0.59 MA). It was found that the Al DPFL plasma on MAIZE was cooler near the anode and hotter near the cathode. Additionally, the Al DPFL plasma on MAIZE was found to be optically thin near the anode, a rarity amongst Al plasmas on the Zebra generator [8, 20].

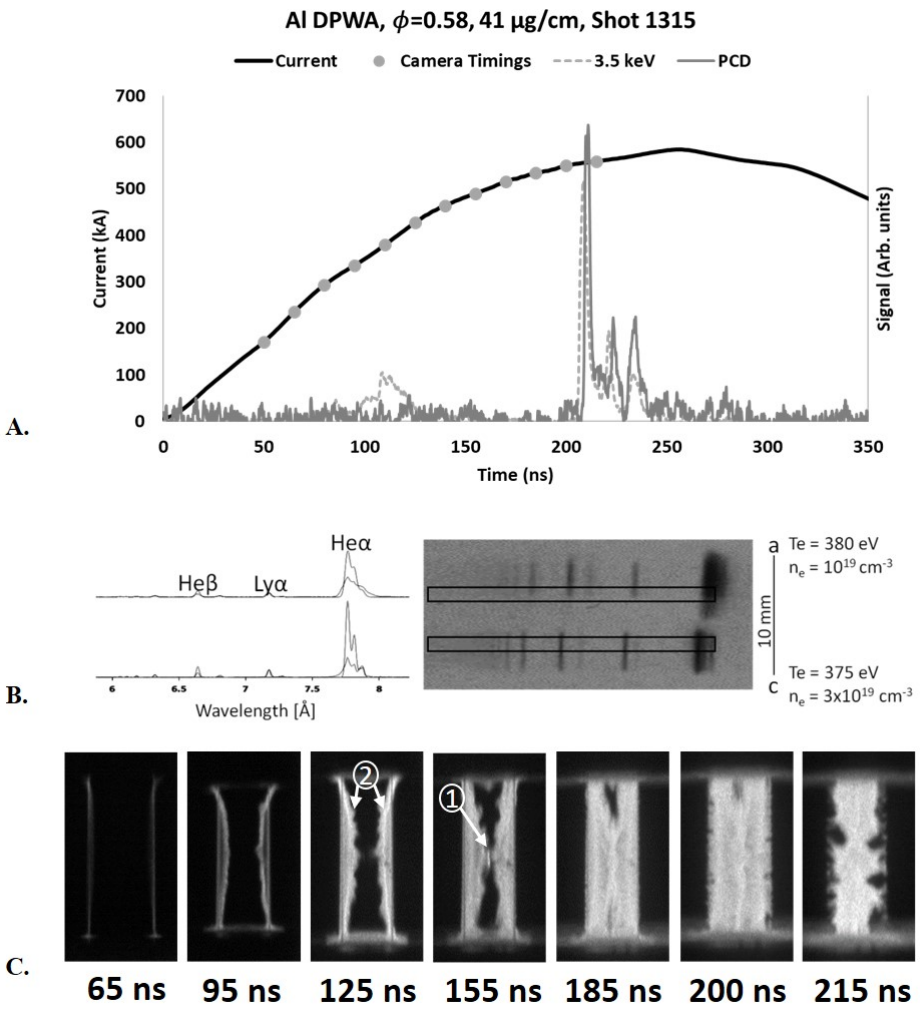

Figure 4. Al DPWA from MAIZE Shot 1315 (N=6/6, inter-planar gap = 6 mm, inter-wire gap = 0.7 mm, aspect ratio ϕ=0.58, mass = 41 µg/cm). A. The PCD signal (dark grey) shows radiation in the >2.4 keV band, while the Si-diode signal (grey dashes) shows radiation in the >1.4 keV band. The current pulse (black) had a risetime of 260 ns with the implosion occurring at 205-215 ns from the start of current. Grey dots correspond to moments when a self-emission image was taken. B. The 1D spatially resolved, time integrated X-ray spectra are compared to theoretical modelling to find plasma conditions. C. Self-emission images showing the implosion evolution in time from the start of current. The formation and position of the primary precursor is marked by "1," and the formation of the standing shocks is marked by "2."

IIIc. Radiative Properties of W DPWAs on the MAIZE LTD

In addition to Al DPWAs, W DPWAs were imploded to examine how a higher-atomic-number wire load performs on the MAIZE LTD. The W DPWA successfully imploded, which again presented the first results of its kind on a low-impedance LTD generator [16]. The diameter of the W wires was chosen such that the mass of the W DPWAs (61-76 μg/cm) would be comparable to the Al DPWAs. The most massive of such W DPWAs (76 μg/cm, MAIZE Shot 1334) was used here as the closest comparison in mass and aspect ratio to the high mass Al DPFL (although the DPFL was still a factor of ~4 higher in mass). The W DPWA implosion was characterized by a well-defined signal from the x-ray burst, with a sharp main peak on the PCD (>2.4 keV) signal of 25-30 ns duration, followed by a 25-30 ns secondary burst, in which the plasma load was still radiating, but with lower power (Fig. 5A). Radiation in the >1.4 keV region begins emitting earlier than the main radiation burst (approximately 80 ns), which corresponds to the formation of the precursor column and standing shocks, as can be seen in the self-emission images of Fig. 5B. A peak in the >1.4 keV region occurred at approximately 140 ns, which directly corresponds to a noticeable increase in self-emission brightness of the precursor column. The PCD signal (>2.4 keV) and the Si-diode signal (>1.4 keV) show two distinct peaks in that same time period (the PCD around 110 ns and the >1.4 keV around 100 ns

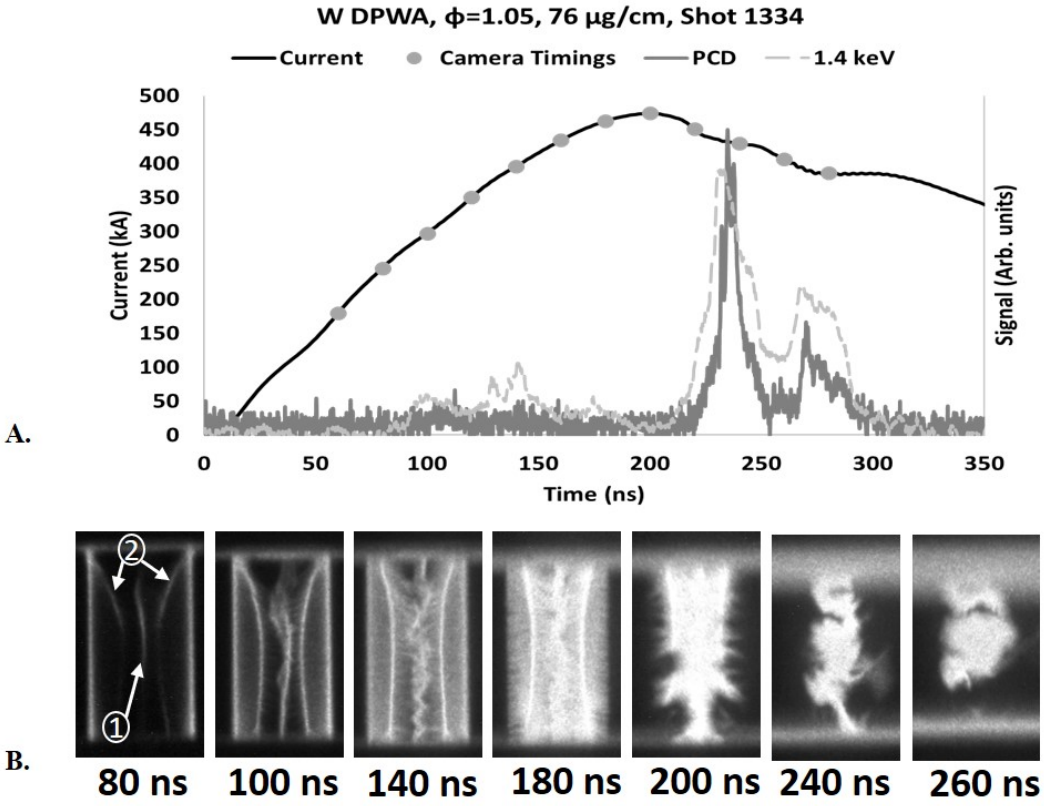

Figure 5. W DPWA from MAIZE Shot 1334 (N=10/10, inter-planar gap = 6 mm, inter-wire gap = 0.7 mm, aspect ratio ϕ=1.05, mass = 76 μg/cm). A. The PCD signal (dark grey) shows radiation emission in >2.4 keV band, while the Si-diode signal (light grey dashes) shows radiation emission in the >1.4 keV band. The current pulse (black) had a risetime of 200 ns with the implosion occurring at 235-245 ns from the start of current. Grey dots indicate camera timings for self-emission images. B. Self-emission images from MAIZE Shot 1334 showing the implosion evolution in time from the start of current. The formation and position of the primary precursor is marked by "1," and the formation of the standing shocks is marked by "2."

and 140 ns). The x-ray yield in the >2.4 keV region of the W DPWA was 1.6 J, and $\varepsilon_{W\ DPWA}$ = 2.1 x 10^{-4}, far larger than the Al DPFLs and DPWAs tested.

IIId. Brief Discussion of MAIZE LTD Performance

The implosion dynamics of loads on the MAIZE LTD are heavily dependent upon LTD machine performance. Table 2 illustrates this by showing the differences in peak current, current risetime, and implosion time of similar and identical Al DPWA loads imploded on MAIZE in different campaigns. When compared to the measurements taken throughout the 2016 campaign, the shots performed during the 2017 campaign are characterized by a slightly higher average peak current, a longer average current risetime, and a much shorter average load implosion time. On average, the peak of x-ray emission occurred nearly 100 ns earlier in the 2017 campaign than in the 2016 campaign. The variation between the 2016 and 2017 campaigns is not fully understood, but we believe that machine performance likely played a significant role (i.e., some of MAIZE's 40 switches were likely firing late and thus asynchronously). Based on an analysis of the data, these performance inconsistencies were likely present during the 2017 campaign, as the variation in switch firing time likely led to the implosions occurring earlier in time. Nevertheless, we note that the shots performed within a given campaign were reproducible and reliable. Therefore, in an effort to minimize the variance in data due to machine performance, all shot comparisons in this article were performed using shots taken in the 2017 campaign, as DPFL experiments were only performed during this campaign.

MAIZE Shot	Campaign	Material	Diameter (μm)	Load Type	Number	Interwire Gap (mm)	Interplanar Gap (mm)	Aspect Ratio	Mass (μg/cm)	Current (kA)	Current Risetime (ns)	Implosion Time (ns)
1311	2017	Al	15	DPWA	8/8	1	3	2.33	76	490	195	80
1313	2017	Al	12.7	DPWA	8/8	1	6	1.17	55	545	325	140
1314	2017	Al	12.7	DPWA	6/6	1	3	1.67	41	590	260	120
1315	2017	Al	12.7	DPWA	6/6	0.7	6	0.58	41	585	260	220
1239	2016	Al	15	DPWA	6/6	1	3	1.67	57	535	275	200
1242	2016	Al	15	DPWA	8/8	1	3	2.33	76	535	275	220
1257	2016	Al	12.7	DPWA	8/8	0.7	6	0.82	55	510	215	260
1258	2016	Al	12.7	DPWA	8/8	1	6	1.17	55	555	215	250

Table 2. Selected Al DPWAs from experimental campaigns on MAIZE in 2016 and 2017. Issues with LTD switch firing times and inconsistent B-dot probe readings apply an estimated error of order 50 kA to the peak current values listed.

IV. Dynamic Load Inductance

As the MAIZE LTD driver is a low-impedance (0.1 Ω) machine, the current trace throughout the implosion is strongly dependent upon the load inductance, which changes throughout the implosion. Combined with a proper understanding of the driver and transmission line circuit parameters, this dependence allows us to extract information about the time evolution of the inductance of a load from a measurement of current. Understanding the behavior of the inductance will help us to better optimize future loads as well as measure the strength of the pinch. To calculate time-dependent inductance, we first find the initial inductance of the load. The initial inductance of each load is determined from calculations of the partial self-inductance of each wire/foil, the partial mutual inductance between each wire/foil, and the partial mutual inductance between each wire/foil and the six axial return posts of the load hardware. Other partial mutual inductances vary negligibly between shots and are accounted for in the series inductance of the load adapter hardware in the MAIZE circuit model. Changing the wire radii or foil thicknesses (as opposed to positions) in these calculations produced minimal changes in the load inductance (<0.3% for factor of two expansion). Therefore, the wire/foil explosion prior to the pinch is assumed to have a negligible effect on the inductance, so the load inductance prior to bulk motion of load material is taken to be constant [16, 24]. Under these simplifying assumptions, we match the portion of the measured current in which the current is rising and when the load is in the plasma phase, but has not yet begun pinching, to a simulated current pulse using the initial load inductance to find a suitable time-averaged resistance of the load at the onset of radiation emission. The time at which the load enters the plasma phase can be seen on the measured current trace as a "notch" in which the slope of the measured current trace lowers, around 30-50 ns after the start of current; this timing is also typical of calculated ablation times using temperature-dependent resistivity and integrated electrical power [28].

Using the calculated initial load inductance and characteristic resistance, a simulated current is calculated in which the pinch does not occur and the load is static. In previous calculations [16, 24], the time-dependent inductance was calculated by finding the difference in the simulated and measured traces, and computing

$$L(t) = L(0)\frac{I_{sim}^2}{I_{meas}^2}, \tag{1}$$

where L(t) is the *effective* time-dependent inductance associated with the total driver-load circuit, L(0) is the initial inductance of the circuit prior to the start of current, I_{sim} is the simulated current pulse, and I_{meas} is the measured current pulse. However, this effective inductance ignores the power associated with the mechanical energy driving the load implosion [29]. Therefore, a modified calculation was implemented to solve for the inductance iteratively which accounts for this energy-transfer mechanism and more closely approximates the true load inductance as a function of time. In this method, the initial guess for L(t) is calculated in the previous manner, but the notation is changed to allow for future iterations,

$$L(t) = L(0)\frac{I_{sim}^2}{I_{meas}^2} \Rightarrow L(t) = \frac{L_0 I_{sim\_0}^2}{I_{meas}^2} = \frac{2E_0}{I_{meas}^2}, \tag{2}$$

where E_0 is the energy stored in the magnetic field. Then, we calculate the implied change in the electromagnetic energy stored in the cavity as a function of time,

$$\Delta E(t) = -\frac{1}{2}\int \frac{dL_i}{dt} I_{meas}^2 \, dt \ , \tag{3}$$

and L is then recalculated by,

$$L_{i+1}(t) = \frac{2(E_0 + \Delta E(t))}{I_{meas}^2} \ , \tag{4}$$

to get the next iteration. The inductance is then calculated by comparing $L_{i+1}(t)$ and $L_i(t)$, finding the maximum error over the interval of interest, and continuing to iterate with equations (3) and (4) until the error falls below a specified convergence criterion. In these calculations, the convergence criterion used was 0.1 nH. Note that we choose this iterative calculation method rather than numerically solving a nonlinear system of circuit equations for the inductance L(t) because it is less sensitive to calibration errors in the measured current. This time-dependent inductance calculation of the plasma load throughout the pinching process can be considered a measurement of pinch strength. The experimentally determined changes of load inductance on Al and W DPWAs and Al DPFLs exhibited correlations in both magnitude and time with measurements of x-ray bursts on shots that demonstrated strong Al and W plasma pinching processes.

Due to the sensitivity of the MAIZE LTD current pulse to switch jitter and dynamic load inductance, there can be a small, but relatively significant, variance between current risetime and load implosion times of even identical load geometries. This is unlike what is seen on "stiffer," high-impedance machines, where identical load types have highly repeatable implosions, such as data seen on the high-impedance UNR Zebra driver (1.9 Ω). For this reason, we have selected data that demonstrate a strong difference in simulated vs. measured current (i.e. data that demonstrate a large inductance change due to an implosion that is cleanly detected), where these data were also selected from shots with low switch jitter, as determined by risetimes that are within the expected range for the total inductance of the loads and load adapter hardware.

IVa. Dynamic Load Inductance of Al DPFL

As shown in Fig. 6 for the Al DPFL, L(t) is strongly correlated with the timing and relative intensity of x-ray emission, confirming that some pinching took place in the precursor column as early as 90-100 ns after the current began. For the Al DPFL, an initial plasma phase inductance was 1.6 nH at 50 ns. As the load begins to implode and material flows towards the center of the load, the difference between the simulated and measured current becomes greater, with the measured current becoming less than the simulated, which corresponds to a rise in inductance. As material begins to form a central precursor column and pinching processes start to occur (Fig. 3C), the inductance rises reaches a local peak (Fig. 6B). The start of radiation emission can be seen to correlate in time with the beginning of the rise in inductance, beginning around 80-90 ns, just around the time when the simulated and measured current traces begin to diverge. The first and greatest maximum in load inductance occurs at 115-125 ns, reaching a maximum inductance of 3.5 nH; this first peak corresponds to the first radiation burst in the >3.5 keV band; the following x-ray burst is likely due to the increase in radiation of the central precursor column, which occurs before the bulk foil material has imploded (as can be seen in

the self-emission images in Fig. 3C). The inductance peaks at 160-170 ns and at 180-190 ns correlate to bulk foil implosion and weaker x-ray bursts, which are more pronounced in the >3.5 keV signal. The inductance then proceeds to decrease as the pinching process comes to an end, at 245-255 ns, making for a total implosion and x-ray emission duration of >150 ns.

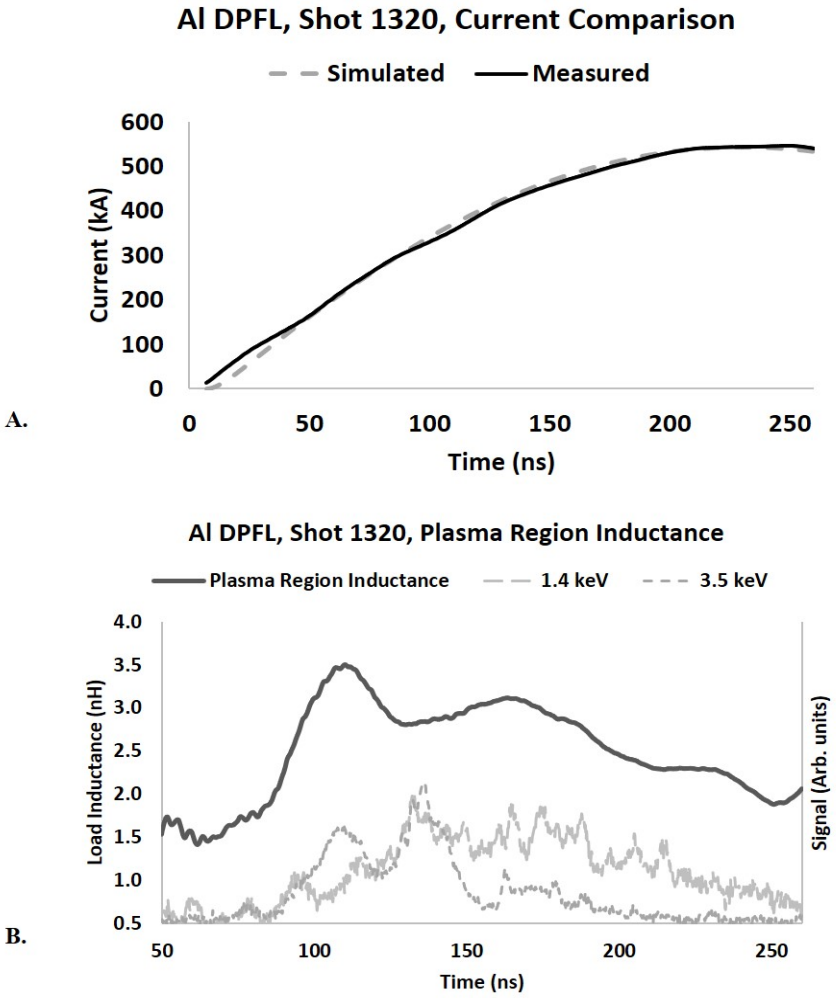

Figure 6. Al DPFL from MAIZE Shot 1320 (inter-planar gap = 3 mm, planar width = 3.5 mm, aspect ratio ϕ=1.17, mass = 55 µg/cm). A. Comparison of simulated current (grey dashes) to the experimentally measured current (black). B. Time-dependent load plasma region inductance throughout the implosion (thick dark grey), plotted with >1.4 keV (light grey longer dashes) and >3.5 keV (grey shorter dashes) x-ray signals.

IVb. Dynamic Load Inductance of Al DPWA

Figure 7 shows the inductance modeling for MAIZE Shot 1315. For the AL DPWA (MAIZE Shot 1315), an initial plasma phase inductance was 1.8 nH at 50 ns. As can be seen from both the current trace and inductance calculations in Fig. 7, the Al DPWA had different implosion characteristics from those of the Al DPFL presented in Fig. 6. By examining the simulated vs. measured current in Fig. 7, we see that the measured current begins to deviate at 80-90 ns, which corresponds with the formation of the standing shocks (Fig. 4C) and the slight production of radiation in the >3.5 keV band (Fig. 7B), concurrent with a noticeable increase in the brightness of the self-emission images from 95-125 ns (Fig. 4C), and corresponds to the initial peak in inductance at 105-115 ns (Fig. 7B). The maximum peak in the inductance history (corresponding to the main x-ray burst) was 4.5 nH, which is nearly 30% higher than the maximum inductance of the Al DPFL. Although the duration of the increasing plasma load inductance (~80 ns) appears more drawn out than the duration of the radiation burst (~40 ns), the maximum inductance still corresponded well in time with the main x-ray burst (at 205-215 ns). In contrast to the Al DPFL, which had an initial rise to its peak of inductance and then a steady decline, the Al DPWA demonstrated an initial rise in inductance correlating to the formation of the standing shocks, before a momentary decline, and then another rise to the peak inductance, correlating to the main pinch and maximum x-ray burst. Also, a higher peak inductance generally correlates to a higher x-ray yield (see Table 1).

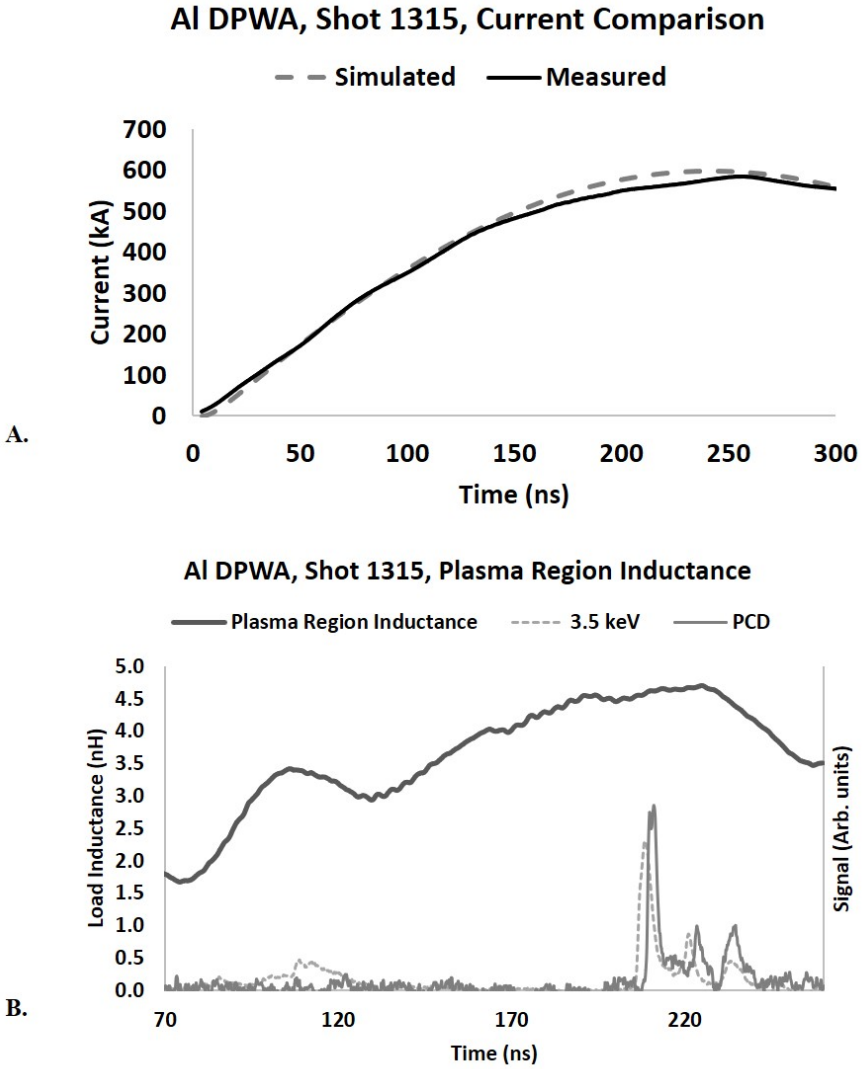

Figure 7. Al DPWA from MAIZE Shot 1315 (N=6/6, inter-planar gap-6 mm, inter-wire gap-0.7 mm, aspect ratio ϕ=0.58, mass-41 µg/cm). A. Comparison of simulated current (grey dashes) to the experimentally measured current (black). B. Time-dependent load plasma region inductance throughout the implosion (thick dark grey), graphed with PCD (dark grey) and >3.5 keV (grey dashes) x-ray signals.

IVc. Dynamic Load Inductance of W DPWA

The W DPWA (Fig. 8) imploded after peak current. As expected, the maximum inductance peak is strongly correlated with the main x-ray radiation burst. For the W DPWA (MAIZE Shot 1334), an initial plasma phase inductance was 3.8 nH at 50 ns. At 220-230 ns, the inductance history reaches a local plateau of 7 nH, which correlates with the peak in x-ray emission. At 265-275 ns, the inductance history reaches its peak value of 9 nH, which correlates with the smaller, secondary peak of the main x-ray burst.

Of all the load configurations tested, the W DPWA had the largest inductance at the time of the pinch. This implies more current transfer to the central pinch column and thus a stronger pinch. This is further supported by the x-ray emission measurements in which the W DPWA radiated 25x more energy than the Al DPWA and DPFL. The total duration of primary radiation emission was approximately 60 ns, which corresponds well with the duration of the peak inductance, seen in Fig. 8B. The time-dependent inductance of the W DPWA performed similarly to the Al DPWA, in that we see an initial rise in inductance corresponding to an early x-ray burst in the >3.5 keV band, proceeded by a momentary lowering before the inductance rises again to its peak value corresponding to the main pinch and x-ray burst. The W DPWA loads also proved to be very reproducible (for a more detailed description of the implosion dynamics of W DPWAs on the MAIZE LTD, see Ref. [16]).

Both the Al DPFL and the Al DPWA reached peak inductance prior to maximum current. Also, the maximum inductance of the Al DPFL was lower than both the Al DPWA and the W DPWA, implying less current transfer to the central column and thus weaker pinching. However, the duration of occurrences of local maxima throughout the primary x-ray emission period for the Al DPFL (135-145 ns) was longer than in the Al DPWA and the W DPWA experiments. This is reflected in the longer emission duration seen in Fig. 3A and Fig. 6B. The Al DPWA demonstrated a stronger pinch than the Al DPFL, while the W DPWA demonstrated the strongest pinch overall, reaching a maximum inductance of 9 nH. For all of the loads tested, the time-dependent plasma inductance was strongly correlated (in both timing and magnitude) with the measured x-ray signals.

These inductance calculations, coupled with the x-ray emissions presented in Section III, showcase the differences in the implosion dynamics of the tested Al DPFLs, Al DPWAs, and W DPWAs. The Al and W DPWAs demonstrated multiple quick X-ray bursts with one main pinch, whereas the Al DPFL exhibited slower material movement producing long-duration emission at low intensity. It should be noted that the peak of the plasma region inductance came at the start of x-ray emission for the Al DPFL (around 100 ns), whereas the peak plasma region inductance for the Al and W DPWAs occurred with the primary pinch and nearer to the peak of the current (around 200 ns for the Al DPWA and around 250 ns for W DPWA).

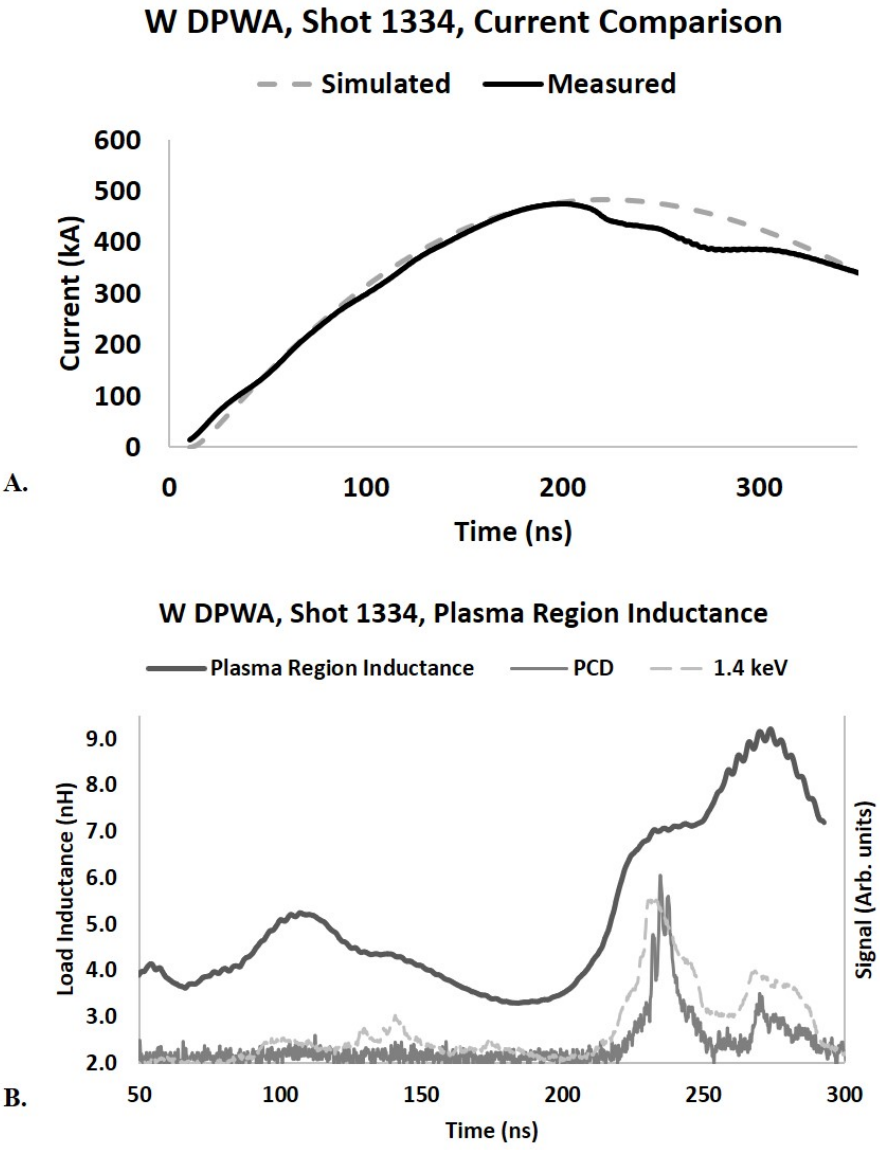

Figure 8. W DPWA from MAIZE Shot 1334 (N=10/10, inter-planar gap = 6 mm, inter-wire gap = 0.7 mm, aspect ratio ϕ=1.05, mass = 76 µg/cm). A. Comparison of simulated current (grey dashes) to the experimentally measured current (black). B. Time-dependent load plasma region inductance throughout the implosion (thick dark grey), plotted with the PCD x-ray signal (dark grey) and the >1.4 keV Si-diode x-ray signal (light grey long dashes).

V. Conclusions

It was predicted that LTD generators allow for greater efficiency than previous machines designed around Marx bank technology [13, 14]. In order to measure the efficiency, the x-ray yield must be measured. The x-ray yield of the more massive Al DPFL, the less massive Al DPWA, and the W DPWA were measured using the absolutely calibrated PCD x-ray detector. In these experiments on the MAIZE LTD generator, the x-ray yield in the >2.4 keV band of the more massive Al DPFL was 3.3 x 10^{-2} J, and thus the conversion efficiency was $\varepsilon_{Al\ DPFL}$ = 4.2 x 10^{-6}. The optimized, less massive Al DPWA was only twice as large at 6.7 x 10^{-2} J, and thus $\varepsilon_{Al\ DPWA}$ = 8.5 x 10^{-6}. Spectroscopic modelling of both the Al DPFLs and Al DPWAs showed comparable electron temperatures (T_e) and densities (n_e): $T_{e,}^{DPFL}$ = 310-340 eV, $n_{e,}^{DPFL}$ = (1-5) x 10^{19} cm^{-3} (I = 0.56 MA), and $T_{e,}^{DPWA}$ = 375-380 eV, $n_{e,}^{DPWA}$ = (1-3) x 10^{19} cm^{-3} (I = 0.59 MA). Additionally, the Al DPWA was found to be optically thin near the anode, in contrast to typical Al plasmas on the Zebra generator [8, 20]. Also, the electron temperature was measured to be hotter near the cathode and cooler near the anode. The W DPWA was the strongest radiator by far, with the total energy emission (1.6 J) and efficiency ($\varepsilon_{W\ DPWA}$ = 2.1 x 10^{-4}) being almost 25 times higher than the Al DPWA on the MAIZE machine.

The result of the heavy, mass-unoptimized Al DPFL producing a comparable overall x-ray output to the mass-optimized Al DPWA, suggests that a mass-optimized DPFL could perform as well as, if not better than, a DPWA of similar mass. This would suggest that DPFLs could still serve as promising replacements for wire array configurations, as was theorized in Ref. [5], but more experiments are needed to say for sure.

Both the Al DPFL and the Al DPWA reached peak inductance prior to maximum current. The maximum load inductance of the Al DPFL never reached as high of a peak as the Al and W DPWAs, implying less current transfer to the central plasma column and thus weaker pinching. The duration of occurrences of local maxima throughout the primary x-ray emission period last much longer in the Al DPFL experiments than in the Al DPWA and W DPWA experiments. The Al DPWA reached a maximum load inductance of 4.5 nH and an x-ray yield of 67 mJ, implying a stronger pinch than the Al DPFL, which reached a maximum inductance of 3.5 nH and a >2.4-keV x-ray yield of 33 mJ. The W DPWA demonstrated the strongest pinch overall, reaching a maximum load inductance of 9 nH (slightly after peak current) and a >2.4-keV x-ray yield of 1.6 J. The time-dependent inductance histories of all three loads tested were strongly correlated with the waveforms from the measured x-ray emissions. These promising results warrant future studies of both foil liners and wire arrays on LTD generators and will help in optimizing future load configurations. We note in particular that the longer emission history from the DPFL could be useful for x-ray pulse shaping applications, if we can demonstrate better control over the waveform in future experiments. This will require significant computational design work as well as experimental validation.

VI. Acknowledgments

This work was supported by the NNSA under DOE grants DE-NA0003047 and DE-NA0003877. Sandia National Laboratories is a multimission laboratory managed and operated by National Technology and Engineering Solutions of Sandia, LLC, a wholly owned subsidiary of Honeywell International Inc., for the U.S. Department of Energy's National Nuclear Security Administration under contract DE-NA0003525.

This paper describes objective technical results and analysis. Any subjective views or opinions that might be expressed in the paper do not necessarily represent the views of the U.S. Department of Energy or the United States Government.

VII. Data Availability

The data that support the findings of this study can be made available from the corresponding author upon reasonable request.

VIII. References

1. V. L. Kantsyrev, L. I. Rudakov, A. S. Safronova, A. A. Esaulov, A. S. Chuvatin, C. A. Coverdale, C. Deeney, K. M. Williamson, M. F. Yilmaz, I. Shrestha, N. D. Ouart, and G. C. Osborne, Phys. Plasmas, v. 15, 030704 (2008).

2. B. Jones, D. J. Ampleford, R. A. Vesey, M. E. Cuneo, C. A. Coverdale, E. M. Waisman, M. C. Jones, W. E. Fowler, W. A. Stygar, J. D. Serrano, M. P. Vigil, A. A. Esaulov, V. L. Kantsyrev, A. S. Safronova, K. M. Williamson, A. S. Chuvatin, and L. I. Rudakov, Phys. Rev. Lett., v. 104, 125001 (2010).

3. V. L. Kantsyrev, A. S. Safronova, A. A. Esaulov, K. M. Williamson, I. Shrestha, F. Yilmaz, G. C. Osbourne, M. E. Weller, N. D. Ouart, V. V. Shlyaptseva, L. I. Rudakov, A. S. Chuvatin, and A. L. Velikovich, High Energy Density Phys., v. 5, 115 (2009).

4. V. L. Kantsyrev, A. S. Chuvatin, L. I. Rudakov, A. L. Velikovich, I. K. Shrestha, A. A. Esaulov, A. S. Safronova, V. V. Shlyaptseva, G. C. Osborne, A. L. Astanovitsky, M. E. Weller, A. Stafford, K. A. Schultz, M. C. Cooper, M. E. Cuneo, B. Jones, and R. A. Vesey, Phys. Rev. E, Stat. Phys. Plasmas Fluids Relat. Interdiscip. Top., v. 90, 0631206 (2014).

5. V. L. Kantsyrev, A. S. Chuvatin, A. S. Safronova, L. I. Rudakov, A. A. Esaulov, A. L. Velikovich, I. K. Shrestha, A. Astanovitsky, G. C. Osborne, V. V. Shlyaptseva, M. E. Weller, S. Keim, A. Stafford, and M. Cooper, Phys. Plasmas, v. 21, 031204 (2014).

6. K. M. Williamson, V. L. Kantsyrev, A. A. Esaulov, A. S. Safronova, P. Cox, I. Shrestha, G. C. Osborne, M. E. Weller, N. D. Ouart, and V. V. Shlyaptseva, Phys. Plasmas, v. 17, 112705 (2010).

7. A. S. Safronova, V. L. Kantsyrev, A. A. Esaulov, A. Chuvatin, M. E. Weller, V. V. Shlyaptseva, I. Shrestha, S. F. Kim, A. Stafford, C. A. Coverdale, J. P. Apruzese, N. D. Ouart, and J. L. Giuliani, Phys. Plasmas 21, 031205 (2014).

8. A. S. Safronova, V. L. Kantsyrev, M. E. Weller, V. V. Shlyaptseva, I. K. Shrestha, A. Stafford, M. T. Schmidt-Petersen, M. Y. Lorance, K. A. Schultz, and A. S. Chuvatin, Phys. Plasmas 23, 101210 (2016).

9. A. S. Safronova, V. L. Kantsyrev, A. A. Esaulov, U. I. Safronova, V. V. Shlyaptseva, I. Shrestha, G. C. Osborne, M. E. Weller, A. Stafford, M. Lorance, and A. Chuvatin, Int. J. Mod. Phys., Conf. Ser., v. 32, 1460316 (2014).

10. A. S. Safronova, V. L. Kantsyrev, A. A. Esaulov, N. D. Ouart, V. Shlyaptseva, K. M. Williamson, I. Shrestha, G. C. Osborne, and M. E. Weller, J. Phys.: Conf. Ser. 244, 032031 (2010).

11. M. E. Weller, A. S. Safronova, V. L. Kantsyrev, A. A. Esaulov, I. Shrestha, J. P. Apruzese, J. L. Giuliani, A. S. Chuvatin, A. Stafford, S. F. Keim, V. V. Shlyaptseva, G. C. Osborne, and E. E. Petkov, Phys. Plasmas 21, 031206 (2014).

12. V. L. Kantsyrev, A. S. Chuvatin, L. I. Rudakov, A. L. Velikovich, I. K. Shrestha, A. A. Esaulov, A. S. Safronova, V. V. Shlyaptseva, G. C. Osborne, A. L. Astanovitsky, M. E. Weller, A. Stafford, K. A. Schultz, M. C. Cooper, M. E. Cuneo, B. Jones, and R. A. Vesey, AIP Conference Proceedings (Dense Z pinches 2014), v. 1639, 102 (2014).

13. M. G. Mazarakis, W. E. Fowler, K. L. LeChien, F. W. Long, M. K. Matzen, D. H. McDaniel, R. G. McKee, C. L. Olson, J. L. Porter, S. T. Rogowski, K. W. Struve, W. A. Stygar, J. R. Woodworth, A. A. Kim, V. A. Sinebryukhov, R. M. Gilgenbach, M. R. Gomez, D. M. French, Y. Y. Lau, J. C. Zier, D. M. VanDevalde, R. A. Sharpe, and K. Ward, IEEE Trans. Plasma Sci., v. 38, 704 (2010).

14. W. A. Stygar, T. J. Awe, J. E. Bailey, N. L. Bennett, E. W. Breden, E. M. Campbell, R. E. Clark, R. A. Cooper, M. E. Cuneo, J. B. Ennis, D. L. Fehl, T. C. Genoni, M. R. Gomez, G. W. Greiser, F. R. Gruner, M. C. Herrmann, B. T. Hutsel, C. A. Jennings, D. O. Jobe, B. M. Jones, M. C. Jones, P. A. Jones, P. F. Knapp, J. S. Lash, K. R. LeChien, J. J. Leckbee, R. J. Leeper, S. A. Lewis, F. W. Long, D. J. Lucero, E. A. Madrid, M. R. Martin, M. K. Matzen, M. G. Mazarakis, R. D. McBride, G. R. McKee, C. L. Miller, J. K. Moore, C. B. Mostrom, T. D. Mulville, K. J. Peterson, J. L. Porter, D. B. Reisman, G. A. Rochau, G. E. Rochau, D. V. Rose, D. C. Rovang, M. E. Savage, M. E. Sceiford, P. F. Schmit, R. F. Schneider, J. Schwarz, A. B. Sefkow, D. B. Sinars, S. A. Slutz, R. B. Spielman, B. S. Stoltzfus, C. Thoma, R. A. Vesey, P. E. Wakeland, D. R. Welch, M. L. Wisher, and J. R. Woodworth, Phys. Rev. Special Topics Accel. Beams, v. 18, 110401 (2015).

15. A. S. Safronova, V. L. Kantsyrev, M. E. Weller, V. V. Shlyaptseva, I. K. Shrestha, M. Y. Lorance, M. T. Schmidt-Petersen, A. Stafford, M. C. Cooper, A. M. Steiner, D. A. Yager-Elorriaga, S. G. Patel, N. M. Jordan, R. M. Gilgenbach, and A. S. Chuvatin, IEEE Trans. Plasma Sci., v. 44, No. 4, 432 (2016).

16. V. L. Kantsyrev, A. S. Safronova, V. V. Shlyaptseva , I. K. Shrestha, C. J. Butcher, M. T. Schmidt-Petersen, A. Stafford, A. M. Steiner, D. A. Yager-Elorriaga, P. C. Campbell , S. M. Miller, N. M. Jordan , R. D. McBride , R. M. Gilgenbach, J.L. Giuliani, and A. L. Velikovich, IEEE Trans. Plasma Sci., v. 46, No. 11, 3778 (2018).

17. R. M. Gilgenbach, M. R. Gomez, J. C. Zier, W. W. Tang, D. M. French, Y. Y. Lau, M. G. Mazarakis, M. E. Cuneo, M. D. Johnston, B. V. Oliver, T. A. Mehlhorn, A. A. Kim, and V. A. Sinebryukhov, AIP Conference Proceedings, vol. 1088, 259 (2009).

18. J. P. Knauer, F. J. Marshall, B. Taakobi, D. Anderson, B. A. Schmitt, K. M. Chandler, S. A. Pikuz, T. A. Shelkovenko, M. D. Mitchell, and D. A. Hammer, Rev. Sci. Instrum., v. 77, 10F331 (2006).

19. K. M. Chandler, S. A. Pikuz, T. A. Shelkovenko, M. D. Mitchell, D. A. Hammer, and J. P. Knauer, Rev. Sci. Instrum., v. 76, 113111 (2005).

20. M. F. Yilmaz, A. S. Safronova, V. L. Kantsyrev, A. A. Esaulov, K. M. Williamson, I. K. Shrestha, M. E. Weller, G. C. Osborne, and V. V. Shlyaptseva, High Energy Density Phys., v. 8, 30 (2012).

21. D. A. Yager-Elorriaga, P. Zhang, A. M. Steiner, N. M. Jordan, Y. Y. Lau, and R. M. Gilgenbach, Phys. Plasmas, v. 23, 101205 (2016).

22. D. A. Yager-Elorriaga, P. Zhang, A. M. Steiner, N. M. Jordan, P. C. Campbell, Y. Y. Lau, and R. M. Gilgenbach, Phys. Plasmas, v. 23, 124502 (2016).

23. A. M. Steiner, P. C. Campbell, D. A. Yager-Elorriaga, K. C. Cochrane, T. R. Mattsson, N. M. Jordan, R. D. McBride, Y. Y. Lau, and R. M. Gilgenbach, Phys. Plasmas, v. 25, 032701 (2018).

24. A. M. Steiner, D. A. Yager-Ellorriaga, S. G. Patel, N. M. Jordan, R. M. Gilgenbach, A. S. Safronova, V. L. Kantsyrev, V. V. Shlyapseva, I. K. Shrestha, and M. T. Schmidt-Petersen, Phys. Plasmas, v. 23, 101206 (2016).

25. A. A. Esaulov, A. L. Velikovich, V. L. Kantsyrev, T. A. Mehlhorn, and M. E. Cuneo, Phys. Plasmas, v. 13, 120701 (2006).

26. A. A. Esaulov, V. L. Kantsyrev, A. S. Safronova, A. L. Velikovich, I. K. Shrestha, K. M. Williamson, and G. C. Osborne, Phys. Rev. E, v. 86, 046404 (2012).

27. V. L. Kantsyrev, A. S. Chuvatin, A. A. Esaulov, A. S. Safronova, L. I. Rudakov, A. Velikovich, L. M. Williamson, G. C. Osborne, I. K. Shrestha, M. E. Weller, and V. V. Shlyaptseva, Phys. Plasmas, v. 20, 070702 (2013).

28. A. M. Steiner, Ph.D. Dissertation, University of Michigan, (2016).

29. R. D. McBride, W. A. Stygar, M. E. Cuneo, D. B. Sinars, M. G. Mazarakis, J. J. Leckbee, M. E. Savage, B. T. Hutsel, J. D. Douglass, M. L. Kiefer, B. V. Oliver, G. R. Laity, M. R. Gomez, D. A. Yager-Elorriaga, S. G. Patel, B. M. Kovalchuk, A. A. Kim, P.-A. Gourdain, S. N. Bland, S. Portillo, S. C. Bott-Suzuki, F. N. Beg, Y. Maron, R. B. Spielman, D. V. Rose, D. R. Welch, J. C. Zier, J. W. Schumer, J. B. Greenly, A. M. Covington, A. M. Steiner, P. C. Campbell, S. M. Miller, J. M. Woolstrum, N. B. Ramey, A. P. Shah, B. J. Sporer, N. M. Jordan, Y. Y. Lau, and R. M. Gilgenbach, IEEE Trans. Plasma Sci., v. 46, No. 11, 3928 (2018).